

2019

Segregation of Mo atoms into stacking faults in CrFeCoNiMo alloy

Kaisheng Ming

University of Nebraska-Lincoln, ming@unl.edu

Xiaofang Bi

Beihang University, Beijing, bixf@buaa.edu.cn

Jian Wang

University of Nebraska-Lincoln, jianwang@unl.edu

Follow this and additional works at: <https://digitalcommons.unl.edu/mechengfacpub>

 Part of the [Mechanics of Materials Commons](#), [Nanoscience and Nanotechnology Commons](#), [Other Engineering Science and Materials Commons](#), and the [Other Mechanical Engineering Commons](#)

Ming, Kaisheng; Bi, Xiaofang; and Wang, Jian, "Segregation of Mo atoms into stacking faults in CrFeCoNiMo alloy" (2019).
Mechanical & Materials Engineering Faculty Publications. 388.
<https://digitalcommons.unl.edu/mechengfacpub/388>

This Article is brought to you for free and open access by the Mechanical & Materials Engineering, Department of at DigitalCommons@University of Nebraska - Lincoln. It has been accepted for inclusion in Mechanical & Materials Engineering Faculty Publications by an authorized administrator of DigitalCommons@University of Nebraska - Lincoln.

Segregation of Mo atoms into stacking faults in CrFeCoNiMo alloy

Kaisheng Ming,^{1,2} Xiaofang Bi,¹ and Jian Wang²

¹ Key Laboratory of Aerospace Materials and Performance (Ministry of Education),
School of Materials Science and Engineering, Beihang University, Beijing,
People's Republic of China;

² Mechanical and Materials Engineering, University of Nebraska-Lincoln, Lincoln, USA

Corresponding authors – Jian Wang jianwang@unl.edu; Xiaofang Bi bixf@buaa.edu.cn

ORCID: Jian Wang <http://orcid.org/0000-0001-5130-300X>

Abstract

Solute segregation at dislocations can impede the motion of dislocations, strengthening materials. Here, we study the formation and role of solute segregation at dislocations in CrFeCoNiMo high-entropy alloys (HEAs) by high-angle annular dark-field scanning transmission electron microscopy imaging and mechanical testing both deformed and annealed samples. Mo atoms exhibit pronounced segregation into the planar-extended core of dislocations, i.e. stacking faults, causing the increase in the yield strength while the loss of the ductility. This work suggests that mechanical properties of HEAs can be tailored by alloying additional elements that are in favour of segregation into dislocations.

Keywords: High-entropy alloys, segregation, strengthening, stacking faults

Published in *Philosophical Magazine*, 2019

doi 10.1080/14786435.2019.1569768

Copyright © 2019 Informa UK Limited, trading as Taylor & Francis Group. Used by permission.

Submitted 8 October 2018; accepted 5 January 2019; published 23 January 2019.

1. Introduction

Solute strengthening mechanisms are commonly considered to play a crucial role in strengthening multi-principal elements alloys (often referred to as high-entropy alloys, HEAs). As solid solutions, there is no distinction between solute and solvent atoms [1,2], although HEAs often adopt simple crystal structures, such as face-centered cubic (FCC) or body-centered cubic (BCC) structures [1,3,4]. The distribution of elements may not be completely random, i.e. short range ordering is possible [1], but it is impossible to identify the distribution of various elements by modern microscopies. However, solute segregation at dislocations [5,6] and interfaces [7–9] is a common phenomenon in many metallic alloy systems, which decreases the mobility of dislocations and interfaces and thus makes a significant effect on mechanical properties of materials [10]. This inspires us to study segregation of atoms in HEAs through annealing deformed samples and then measuring mechanical properties. Indeed, it has been shown that equi-atomic single-phase FCC CrMnFeCoNi HEA that was deformed by cold rolling can be hardened by subsequent annealing below the recrystallization temperature [11]. It is conceivable that solute segregation by annealing may be responsible for the increase in hardness. But further work is required to elucidate this point.

The Co-Cr-Fe-Ni HEA system plus the Mo element is chosen for this study. The Co-Cr-Fe-Ni system exhibits a single-phase solid solution with the FCC structure [12]. More importantly, Co-Cr-Fe-Ni alloys plastically deform through slips of $\{111\}(1/2)$ $\langle 110 \rangle$ dislocations and/or twinning associated with successive gliding of $\{111\}$ $(1/6)$ $\langle 112 \rangle$ Shockley partial dislocations [13–16], suggesting a low stacking fault energy (SFE) of $\{111\}$ plane [17,18]. Among the five elements, Mo has the largest metallic radius Ni (0.124 nm), Co (0.125 nm), Fe (0.126 nm), Cr (0.128 nm), Mo (0.139 nm), and thus potentially maximizes solid solution strengthening and impedes the recrystallization and grain growth. In addition, Mo atoms are found to preferentially segregate into grain boundaries in Ni-Mo alloys [8], the matrix/precipitate interfaces in ferritic steels [19] and stacking faults (SFs) in Cu-based solid solution alloys [20,21]. A recent study on Cr-Fe-Co-Ni-Mo system revealed that high composition of Mo (exceeding 10 at. %) would cause the formation of precipitates [22]. In this study, a small amount of Mo, 6 at. % is alloyed with Cr-Fe-Co-Ni.

We fabricate a single FCC-phase $\text{Cr}_{20}\text{Fe}_6\text{Co}_{34}\text{Ni}_{34}\text{Mo}_6$ multi-principal elements alloy by arc-melting and cold rolling. The Co-Cr-Fe-Ni alloy system is chosen for this study. Microstructure characterization of deformed samples reveals that plastic deformation of the cold-rolled alloy is dominated by dislocations with the wide planar-extended core, corresponding to formation of extensive SFs and nano-twins. Combining the annealing and tension testing, we reveal the segregation of Mo atoms into SFs in the CrFeCoNiMo alloy, leading to significant strengthening. The segregation of Mo atoms into SFs is further confirmed by using high-angle annular dark-field scanning transmission electron microscopy.

2. Experiments

Alloy ingots with nominal compositions of $\text{Cr}_{20}\text{Fe}_6\text{Co}_{34}\text{Ni}_{34}\text{Mo}_6$ (at. %) are prepared by arc-melting under an argon atmosphere, subsequently homogenized in vacuum at 1200°C for 48 h and then cooled in the furnace. The synthesized samples are referred to as homogenized-alloys (marked by #1). The homogenized ingots are further hot-rolled at 1100°C to the sheet with a thickness of 8 mm, followed by air-cooling. Before cold-rolling, the hot-rolled strips are immersed in a liquid nitrogen bath for about 10–15 min and immediately cold-rolled to final sheets ~ 2.4 mm in thickness ($\sim 70\%$ thickness reduction). The cold-rolled samples are marked as #2. In order to easily perceive the role of Mo segregation in strengthening materials, our experiments are conducted through three steps. In the first step, we search for the annealing condition which corresponds to the peak strength of cold-rolled samples after annealing. To do so, cold-rolled sheets (#2) are subjected to annealing at $400\text{--}1150^\circ\text{C}$ for 1 h and followed by air cooling (AC). The peak strength happens at an annealing temperature of 500°C . In the second step, we further measure the hardness of the samples that are annealed at 500°C for 0 min–20 h. The samples at an annealing temperature of 500°C show a strength plateau after annealing 1 h. The annealed sample at 500°C for 1 h is denoted by #3. In the third step, we conduct an alternatively anneal and deform process. The #3 sample is slightly cold-rolled again with the 15% thickness reduction (#4), subsequently annealed at 500°C for 1 h again (#5), then slightly cold-rolled again with the 15% thickness reduction

(#6), and finally annealed at 500°C for 1 h (#7). We measure stress-strain responses of these samples by tensile testing at room temperature and characterize microstructure and defects using transmission electron microscopy (TEM).

Vickers hardness measurements are performed using a standard micro-hardness tester and a load of 500 g. Ten points are tested on each sample, and the hardness values are obtained from the averages of these ten values. Flat dogbone-shaped tensile specimens with a gauge length of 18 mm, the thickness of 2 mm and width of 3 mm are machined from samples by electric discharge machining, and are ground through 1200-grit SiC paper. Tensile tests are performed on an INSTRON-8801 instrument at room temperature with a strain rate 10^{-3} s^{-1} . The elongation is measured using the YYJ-5/15-L electronic extensometer. Microstructure characterization is performed by JEM 2100F transmission electron microscopy (TEM) operated at 200 kV and Titan G₂ 60-300 Cs-corrected electron microscope operated at 300 kV. Specimens for TEM observation are thinned using mechanical grinding followed by double-jet electropolishing in a solution of 5% perchloric acid and 95% alcohol at -30°C and an applied voltage of 30 V.

3. Results and discussion

Microstructure characterization reveals that cold-rolling substantially refines the grain size down to nanoscale (Figures 1a,b), and introduces highly dense dislocation walls and large numbers of nano-sized dislocation cells (Figure 1c). The corresponding selected area diffraction (SAED) patterns inserted in Figures 1(a, c) confirm the single-phase FCC structure in cold-rolled samples. The dislocation cell interiors are largely dislocation-free (Figure 1c), but contain numerous SFs as shown in the high-resolution transmission electron microscopy (HR-TEM) image (Figure 1d), indicating a low SFE of the $\text{Cr}_{20}\text{Fe}_6\text{Co}_{34}\text{Ni}_{34}\text{Mo}_6$ alloy at room temperature. The generation of high density of SFs is further confirmed by the presence of streaking along $\langle 111 \rangle$ in the fast Fourier transform (FFT) image inserted in Figure 1(d).

Figures 1(e,g) is the typical TEM micrographs of the cold-rolled sample after tension to fracture, revealing the deformation mechanisms. As shown in Figure 1(e), numerous deformation nano-twins

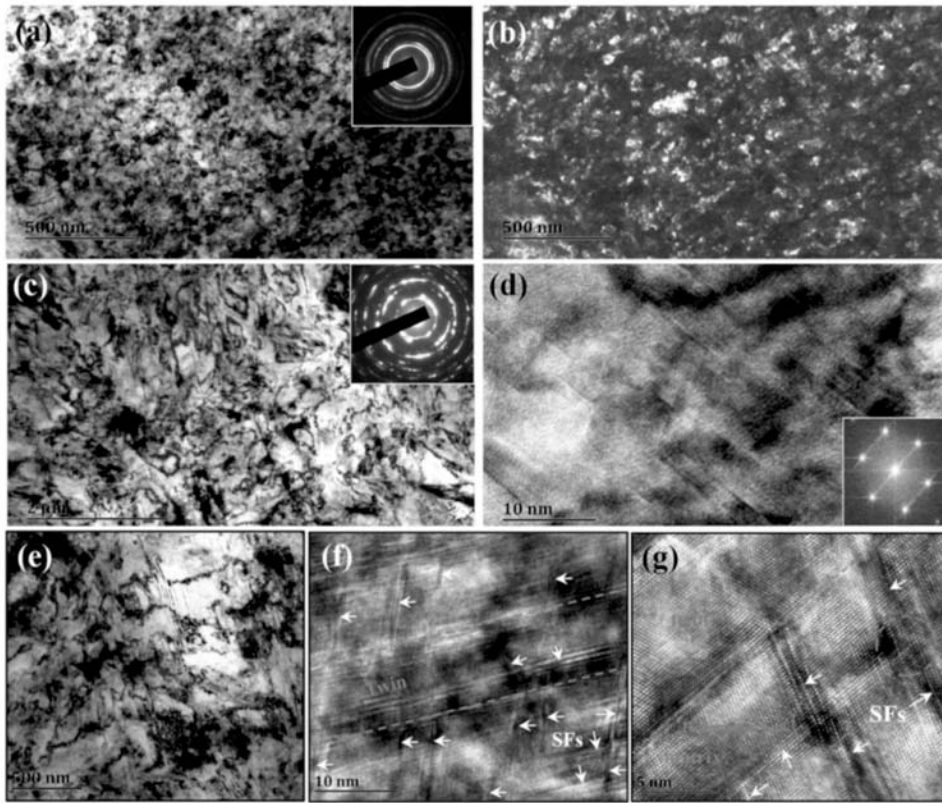


Figure 1. Typical TEM micrographs of the cold-rolled $\text{Cr}_{20}\text{Fe}_6\text{Co}_{34}\text{Ni}_{34}\text{Mo}_6$ alloy (70% thickness reduction) (a-d) before and (e-g) after tension to fracture at room temperature. (a) TEM brightfield (BF) image with the corresponding SAED pattern inset, (b) the corresponding dark-field image; (c) TEM BF image showing dislocation cells and walls, and (d) HRTEM image corresponding to the dislocation cell interior, showing high density of SFs. (e) TEM BF image of the sample after tension to fracture showing nano-twins; (f) and (g) the corresponding HRTEM image showing interactions between twins and SFs. SFs and dislocation locks are indicated by white arrows and red circles, respectively.

are observed, which are connected to several dislocation walls. The formation of deformation twins is ascribed to the pre-existing dislocation walls and the low misorientation across the dislocation wall. In addition, numerous SFs are observed in the dislocation cells (Figures 1f,g), indicating that dislocations in the walls act as sources for emission of Shockley partial dislocations. Under applied stress, leading partials can be emitted from dislocation walls and arrested by another dislocation wall [23]. When trailing partials are pinned by dislocation walls, deformation twins form, especially in fine-scale grains [24,25]. The low misorientation between the adjacent grains across

dislocation walls plays a weak resistance to slip transmission across dislocation walls. Under high applied stress, deformation nanotwins can propagate through several dislocation cells, as shown in Figure 1(e). The HRTEM images of Figures 1(f,g) illustrate the strong interaction of twin boundaries and SFs, leading to the formation of many Lomer-Cottrell locks. These results clearly reveal that plastic deformation in cold-rolled samples is carried over by Shockley partial dislocations, corresponding to formation of extensive SFs and nano-twins during tensile tests.

The cold-rolled samples are subjected to annealing for 1 h at various temperatures, and subsequent hardness testing is conducted to assess the mechanical properties. Figure 2(a) shows the variation of hardness with annealing temperature and grain size. Note that the error bars are smaller than the symbols and therefore invisible. Intriguingly, annealing at modest temperatures of 400–600 °C for 1 h leads to a significant hardening rather than softening, with the hardness increases ranging from 12% to 26%. The maximum hardness of ~690 HV is obtained at the annealing temperature of 500°C. The average grain sizes of the cold-rolled and 400–600°C annealed samples range from 0.3–0.8 μm , without apparent grain growth during modest annealing at below 600 °C. With further increasing annealing temperature (>600 °C), the hardness decreases significantly due to grain growth. The annealing-induced hardening behavior might be attributed to Mo atoms segregation into SFs which will be examined in the following section. As the annealing temperature is lower than

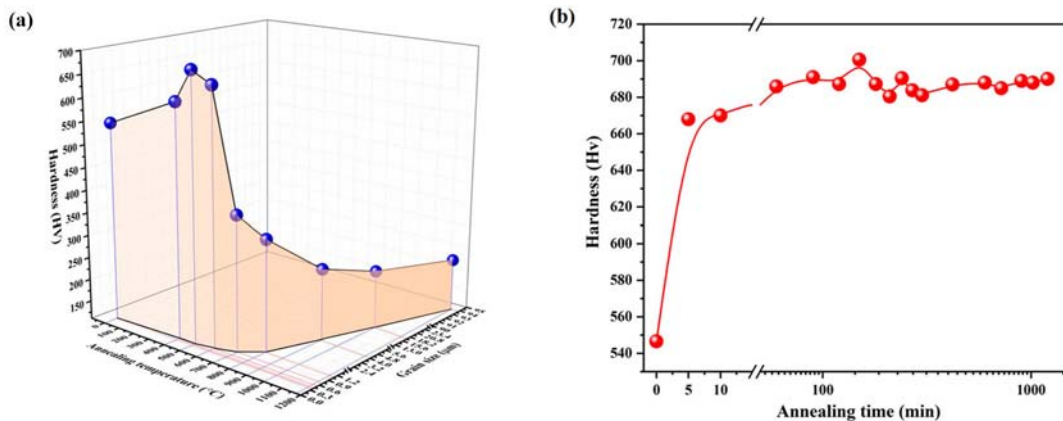


Figure 2. (a) Hardnesses and grain sizes of annealed cold-rolled samples with respect to annealing temperatures; (b) Hardness of 500 °C annealed cold-rolled samples for various annealing times.

500 °C, Figure 2(a) shows that solute hardening is stronger than softening due to grain growth. While above 500 °C, solute hardening is weaker than softening due to grain growth. This offers the best condition (annealing at 500 °C) to reveal the origin of solute hardening. To see how quickly the hardening process occurs, isothermal treatments were performed at a temperature of 500 °C, and the corresponding values of hardness are plotted in Figure 2(b). The hardening occurs very rapidly, the peak hardness is nearly reached within 10 mins. With further increasing annealing time to 20 h, the hardness remains unchanged at approximately 690 HV.

Figure 3 reveals an interesting variation, alternative hardening by annealing (500 °C for 1 h) and softening by slight deformation (15% cold rolling). As shown in Figure 3(a), 1□2 corresponds to that the

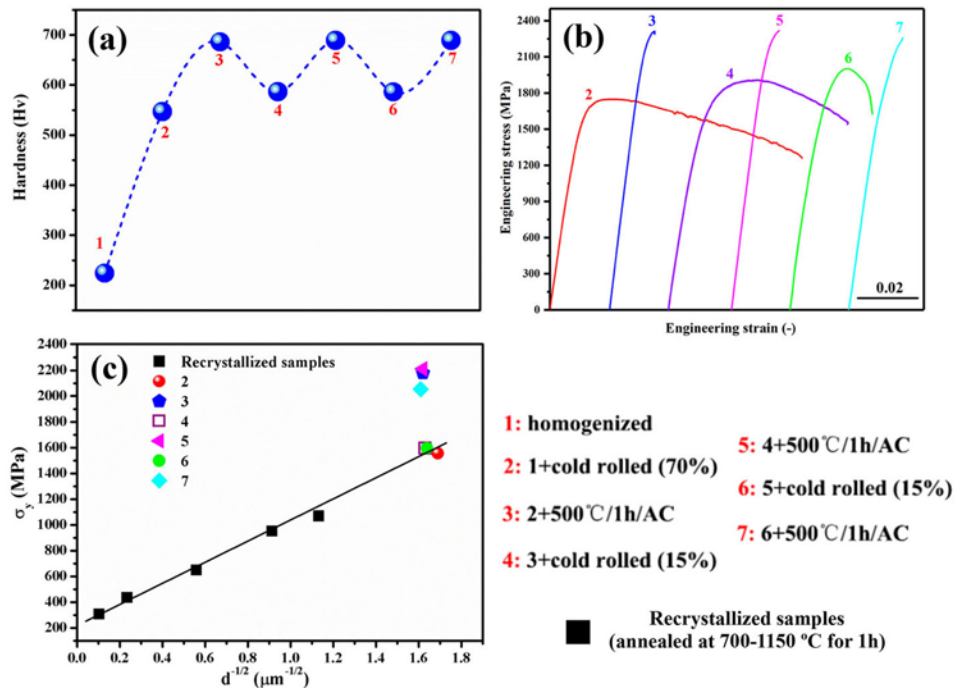


Figure 3. Alternative hardening by annealing (500 °C for 1h) and softening by slight deformation (15% cold rolling). (a) Hardness at various states; (b) room-temperature engineering stress-strain curves at different states. (c) The 0.2% offset yield strength of the recrystallized samples at different states. State 1 is the homogenized alloy; State 2 is that the state 1 sample is cold rolled 70%; State 3 is that the state 2 sample is annealed at 500°C for 1 h; State 4 is that the state 3 sample is deformed 15% by cold rolling; State 5 is that the state 4 sample is annealed at 500 °C for 1h; State 6 is that the state 5 sample is deformed 15% by cold rolling; State 7 is that the state 6 sample is annealed at 500 °C for 1h.

homogenized alloy is cold rolled with 70% thickness reduction. The hardness increases corresponding to work-hardening due to the storage of high density of dislocations, SFs and sub-boundaries by cold-rolling. Interestingly, when the sample is annealed at 500°C for 1 h, annealing-induced hardening happens, corresponding to 2→3. When the 500 °C annealed sample is further cold-rolled with 15% thickness reduction, its hardness is reduced by approximately 15%, corresponding to 3→4 in Figure 3(a). Then, we further carried out alternatively repeated annealing at 500 °C for 1 h and subsequent low level of deformation (15% cold rolling) as well as hardness tests. Repeated hardening by annealing at a modest temperature and softening by slight deformation are observed, corresponding to 4→5→6→7 in Figure 3(a). We also performed room-temperature tensile tests to assess the mechanical response of the annealed and deformed samples. The corresponding tensile curves are plotted in Figure 3(b), curves 2, 4, 6 correspond to cold-rolled samples and curves 3, 5, 7 correspond to 500 °C annealed samples. The results show the enhanced strength and the decrease in the elongation after annealing, and the softening accompanied with the increase in the elongation after slight deformation. In other words, every slight deformation (15% cold rolling) returns the mechanical properties to that of the initial 70% cold-rolled sample (marked by 2), and every modest annealing brings the mechanical properties back to the original level of the 500 °C annealed sample (marked by 3).

We also test the tensile properties of the recrystallized samples (annealed at 700–1150 °C for 1h) and measure average grain sizes (1.2–94 μm). The grain size (d) dependence of yield strength (σ_y) is plotted in Figure 3(c), following the well-known Hall-Petch relationship. Taking the average dislocation cell size as the grain size, we found that the yield strength of cold-rolled samples (marked by 2, 4 and 6 in Figure 3c) lies on the extrapolated Hall-Petch line, which suggests that dislocation cell boundaries are as effective in blocking dislocation motion as the conventional high-angle grain boundaries. However, the yield strength of the 500°C annealed samples (marked by 3, 5 and 7 in Figure 3c) deviates from the Hall-Petch line, reaching up to ~ 2 GPa, which suggests solute strengthening. Slight deformation (15% cold rolling) induces new mobile dislocations and/or makes dislocations escape from solute atmospheres, softening materials. Note that with accumulative annealing and deformation, the number of sessile dislocations increases, the sample 6 exhibits higher strength than that of samples 4 and 2.

The segregation of Mo atoms into SFs is further confirmed by microstructural analysis on the cold-rolled and 500 °C annealed samples using high-angle annular dark-field scanning transmission electron microscopy (HAADF-STEM) imaging. Figure 4(a) shows the typical HAADF-STEM image of the cold-rolled sample after annealing at 500 °C for 1 h. High density of SFs (marked by red arrows) are observed. The corresponding FFT pattern along an $\langle 110 \rangle$ axis in Figure 4(b) shows the streaking along $\langle 111 \rangle$, which further verifies the presence of SFs. Particularly, the HAADF-STEM image shows that SFs exhibit bright lines along $\{111\}$ planes (Figure 4a). Since the contrast in HAADF imaging is proportional to the atomic numbers [26], the bright

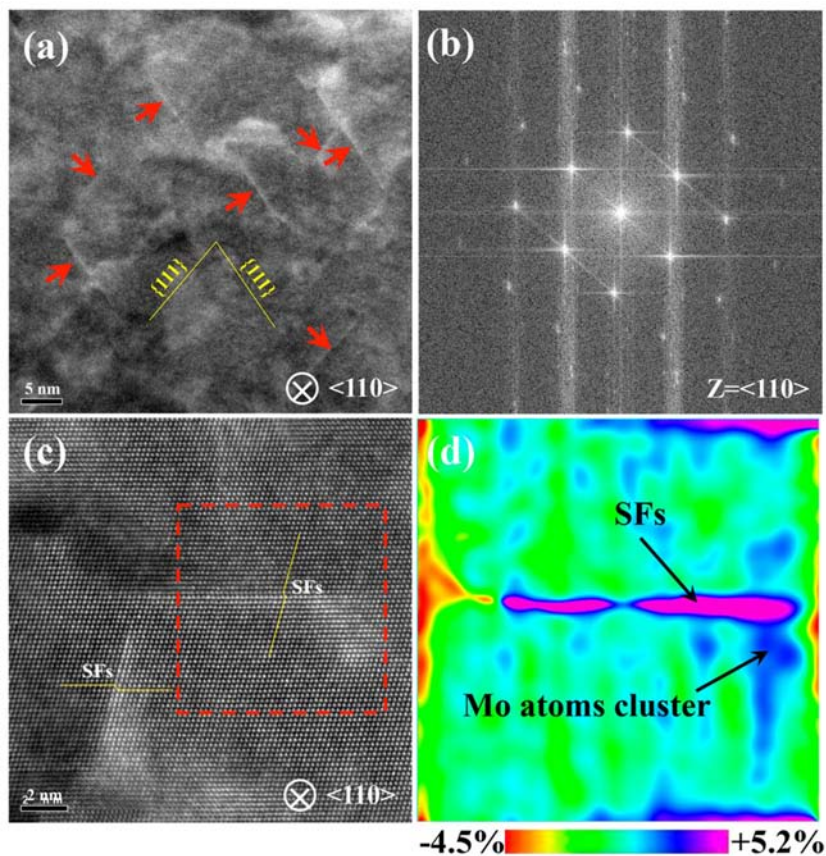


Figure 4. (a) HAADF-STEM image of $\text{Cr}_{20}\text{Fe}_6\text{Co}_{34}\text{Ni}_{34}\text{Mo}_6$ alloy after cold rolling (70%) and annealing at 500 °C for 1 h (corresponding to the sample 3), showing heavier solute atoms (Mo) segregation into SFs (corresponding to bright line marked by red arrows); (b) the corresponding FFT pattern of $\langle 110 \rangle$ axis; (c) HAADF-STEM image and (d) the shear strain map (using the geometrical phase analysis method) of the region outlined by red square in (c), demonstrating the relative strain distribution across the SFs.

atomic columns around SFs are attributed to the heavier Mo atoms, suggesting Mo segregation into SFs. Figure 4(c) is the higher magnification of HAADF-STEM image, showing the SFs along two $\{111\}$ planes and Mo atom clusters around SFs (corresponding to the bright region). The shear strain map (Figure 4d) of the outlined region in Figure 4(c) demonstrates the relative strain changes across the SFs, in which the strain clearly jumps at the SFs and Mo atom clusters owing to the severe local lattice distortion caused by Mo segregation. Mo segregation into SFs and the dislocation depinning from Mo solute atmosphere are further demonstrated by comparing the character of SFs in 500°C annealed sample (corresponding to the sample used to obtain the curve 3 in Figure 3b) and the 15% cold-rolled sample (corresponding to the sample used to obtain the curve 4 in Figure 3b). The HAADF-STEM image (Figure 5a) and atomic column intensity profile (Figure 5b) clearly show that atomic columns around SFs exhibit

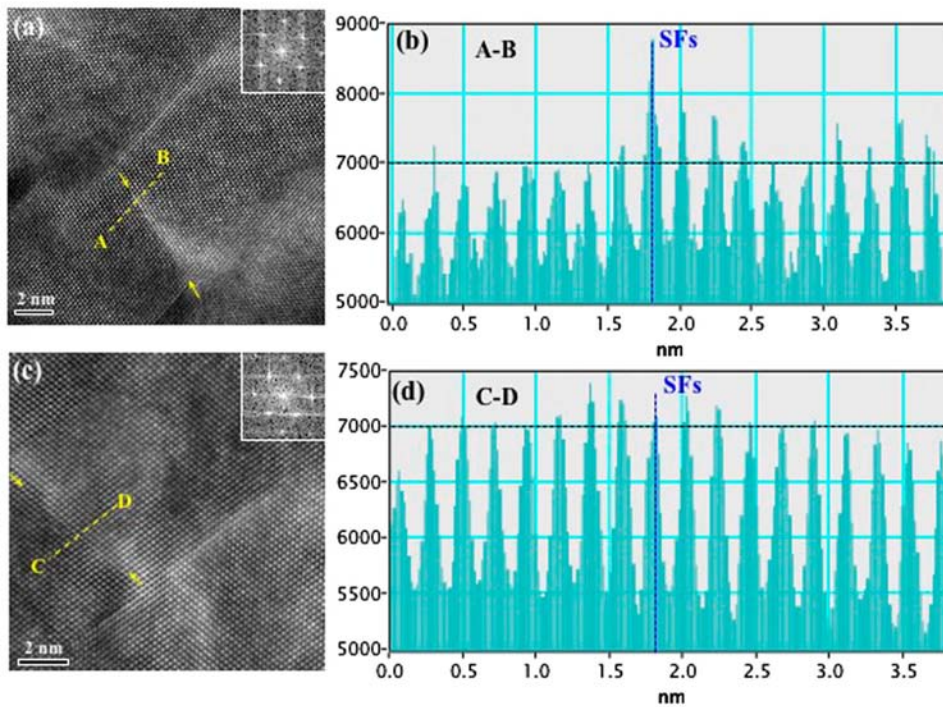


Figure 5. HAADF-STEM image of the $\text{Cr}_{20}\text{Fe}_6\text{Co}_{34}\text{Ni}_{34}\text{Mo}_6$ alloy after (a) cold rolling (70%) and annealing at 500 °C for 1h (corresponding to the sample used to obtain the curve 3 in Figure 3b), and then (c) 15% cold rolling (corresponding to the sample used to obtain the curve 4 in Figure 3b), with the SAED patterns inset. (b) and (d) corresponding atomic column intensity profiles measured from direction AB in (a), and CD in (c), respectively. The SFs regions are marked by yellow arrows in (a) and (c), and green lines in (b) and (d).

strong intensity, demonstrating Mo segregation into SFs in 500°C annealed sample. In contrast, Mo segregation into SFs is not detected in 15% cold-rolled sample, as evidenced by Figures 5(c,d) which show the uniform atomic column intensity around SFs, suggesting that the cold rolling can make dislocations escape from Mo solute atmospheres.

4. Conclusion

$\text{Cr}_{20}\text{Fe}_6\text{Co}_{34}\text{Ni}_{34}\text{Mo}_6$ alloys with a single-phase FCC structure are produced by arc-melting and cold rolling. Cold rolling refines the grain size down to nanoscale and introduces highly dense dislocation walls, large numbers of fine dislocation cells and SFs in cells. The plastic deformation mechanism of the cold-rolled alloy is primarily governed by the movement of Shockley partial dislocations, corresponding to formation of extensive SFs and deformation nanotwins. The segregation of Mo atoms into SFs is characterized by HAADF-STEM imaging, and the role in pinning dislocations is demonstrated by mechanical testing. Through an alternatively anneal and deform process, we demonstrate annealing-induced hardening which is attributed to Mo atoms segregation into SFs and deformation-induced softening which is associated to generation of mobile dislocations and de-pinning of dislocations from the Mo atoms. Our results demonstrate that Mo atoms exhibit pronounced segregation into the planar-extended core of dislocations, i.e. SFs, causing the increase in the yield strength while the loss of the ductility. This work suggests that mechanical properties of HEAs can be tailored by alloying additional elements that are in favour of segregation into structural defects.

Disclosure – No potential conflict of interest was reported by the authors.

Funding – This work is supported by the Science Fund for Creative Research Groups [grant number 61271043]. J.W. acknowledges financial support provided by the Research Council at the University of Nebraska-Lincoln. K.S.M. gratefully acknowledges the financial support for his study in University of Nebraska-Lincoln as a joint PhD student by the China Scholarship Council (File No. 201706020019).

References

- [1] D.B. Miracle and O.N. Senkov, A critical review of high entropy alloys and related concepts, *Acta Mater.* 122 (2017), pp. 448–511.
- [2] I. Toda-Caraballo and P.E.J. Rivera-Díaz-del-Castillo, Modelling solid solution hardening in high entropy alloys, *Acta Mater.* 85 (2015), pp. 14–23.
- [3] Y. Zhang, Y.J. Zhou, J.P. Lin, G.L. Chen and P.K. Liaw, Solid-solution phase formation rules for multi-component alloys, *Adv. Eng. Mater.* 10 (2008), pp. 534–538.
- [4] Z. Wang, Y. Huang, Y. Yang, J. Wang and C.T. Liu, Atomic-size effect and solid solubility of multicomponent alloys, *Scr. Mater.* 94 (2015), pp. 28–31.
- [5] M. Kuzmina, M. Herbig, D. Ponge, S. Sandlobes and D. Raabe, Linear complexes: Confined chemical and structural states at dislocations, *Science* 349 (2015), pp. 1080–1083.
- [6] P. Kontis, Z. Li, D.M. Collins, J. Cormier, D. Raabe and B. Gault, The effect of chromium and cobalt segregation at dislocations on nickel-based superalloys, *Scr. Mater.* 145 (2018), pp. 76–80.
- [7] J.F. Nie, Y.M. Zhu, J.Z. Liu and X.Y. Fang, Periodic segregation of solute atoms in fully coherent twin boundaries, *Science* 340 (2013), pp. 957–960.
- [8] J. Hu, Y. Shi, X. Sauvage, G. Sha and K. Lu, Grain boundary stability governs hardening and softening in extremely fine nanograined metals, *Science* 355 (2017), pp. 1292–1296.
- [9] Z.R. Zeng, Y.M. Zhu, M.Z. Bian, S.W. Xu, C.H.J. Davies, N. Birbilis and J.F. Nie, Annealing strengthening in a dilute Mg–Zn–Ca sheet alloy, *Scr. Mater.* 107 (2015), pp. 127–130.
- [10] P. Lejček, M. Šob and V. Paidar, Interfacial segregation and grain boundary embrittlement: An overview and critical assessment of experimental data and calculated results, *Prog. Mater. Sci.* 87 (2017), pp. 83–139.
- [11] F. Otto, N.L. Hanold and E.P. George, Microstructural evolution after thermomechanical processing in an equiatomic, single-phase CoCrFeMnNi high-entropy alloy with special focus on twin boundaries, *Intermetallics* 54 (2014), pp. 39–48.
- [12] Z. Wu, H. Bei, G.M. Pharr and E.P. George, Temperature dependence of the mechanical properties of equiatomic solid solution alloys with face-centered cubic crystal structures, *Acta Mater.* 81 (2014), pp. 428–441.
- [13] K. Ming, X. Bi and J. Wang, Realizing strength-ductility combination of coarse-grained $\text{Al}_{0.2}\text{Co}_{1.5}\text{CrFeNi}_{1.5}\text{Ti}_{0.3}$ alloy via nano-sized, coherent precipitates, *Int. J. Plast* 100 (2018), pp. 177–191.
- [14] W.H. Liu, Z.P. Lu, J.Y. He, J.H. Luan, Z.J. Wang, B. Liu, Y. Liu, M.W. Chen and C.T. Liu, Ductile CoCrFeNiMo x high entropy alloys strengthened by hard intermetallic phases, *Acta Mater.* 116 (2016), pp. 332–342.
- [15] K. Ming, X. Bi and J. Wang, Microstructures and deformation mechanisms of $\text{Cr}_{26}\text{Mn}_{20}\text{Fe}_{20}\text{Co}_{20}\text{Ni}_{14}$ alloys, *Mater. Charact.* 134 (2017), pp. 194–201.

- [16] A.H. B. Gludovatz, D. Catoor, E.H. Chang, E.P. George, R.O. Ritchie, A fracture-resistant high-entropy alloy for cryogenic applications, *Science* 345 (2014), pp. 1153-1158.
- [17] M. Beyramali Kivy and M. Asle Zaeem, Generalized stacking fault energies, ductilities, and twinnabilities of CoCrFeNi-based face-centered cubic high entropy alloys, *Scr. Mater.* 139 (2017), pp. 83-86.
- [18] S. Zhao, G.M. Stocks and Y. Zhang, Stacking fault energies of face-centered cubic concentrated solid solution alloys, *Acta Mater.* 134 (2017), pp. 334-345.
- [19] N.Q. Vo, C.H. Liebscher, M.J.S. Rawlings, M. Asta and D.C. Dunand, Creep properties and microstructure of a precipitation-strengthened ferritic Fe-Al-Ni-Cr alloy, *Acta Mater.* 71 (2014), pp. 89-99.
- [20] J.M. Popplewell and J. Crane, Order-strengthening in Cu-Al alloys, *Metall. Mater. Trans.* 2 (1971), pp. 3411-3420.
- [21] J.M. Vitek and H. Warlimont, The mechanism of anneal hardening in dilute copper alloys, *Metall. Trans. A* 10 (1979), pp. 1889-1892.
- [22] K. Ming, X. Bi and J. Wang, Precipitation strengthening of ductile Cr 15 Fe 20 Co 35 Ni 20 Mo 10 alloys, *Scr. Mater.* 137 (2017), pp. 88-93.
- [23] L. Liu, Q. Ding, Y. Zhong, J. Zou, J. Wu, Y.-L. Chiu, J. Li, Z. Zhang, Q. Yu and Z. Shen, Dislocation network in additive manufactured steel breaks strength-ductility trade-off, *Mater. Today* 21 (2018), pp. 354-361.
- [24] V. Yamakov, D. Wolf, S. Phillpot and H. Gleiter, Deformation twinning in nanocrystalline Al by molecular-dynamics simulation, *Acta Mater.* 50 (2002), pp. 5005-5020.
- [25] J. Wang and H. Huang, Shockley partial dislocations to twin: Another formation mechanism and generic driving force, *Appl. Phys. Lett.* 85 (2004), pp. 5983-5985.
- [26] K.W. Urban, Studying atomic structures by aberration-corrected transmission electron microscopy, *Science* 321 (2008), pp. 506-510.